



Article

Performance Study of Direct Integration of Phase Change Material into an Innovative Evaporator of a Simple Vapour Compression System

Boniface Dominick Mselle, David Vérez, Gabriel Zsembinski, Emiliano Borri  and
Luisa F. Cabeza * 

GREiA Research Group, Universitat de Lleida, 25001 Lleida, Spain; boniface.mselle@udl.cat (B.D.M.); david.verrez@udl.cat (D.V.); gabriel.zsembinski@udl.cat (G.Z.); emiliano.borri@udl.cat (E.B.)

* Correspondence: luisaf.cabeza@udl.cat; Tel.: +34-973-003576

Received: 30 May 2020; Accepted: 2 July 2020; Published: 5 July 2020



Featured Application: Experimental testing of a novel heat exchanger embedded with thermal energy storage material for refrigeration cycles and air-conditioning systems applications.

Abstract: This paper experimentally investigates the direct integration of 3.15 kg of phase change materials (PCM) into a standard vapour compression system of variable cooling capacity, through an innovative lab-scale refrigerant-PCM-water heat exchanger (RPW-HEX), replacing the conventional evaporator. Its performance was studied in three operating modes: charging, discharging, and direct heat transfer between the three fluids. In the charging mode, a maximum energy of 300 kJ can be stored in the PCM for the cooling capacity at 30% of the maximum value. By doubling the cooling power, the duration of charging is reduced by 50%, while the energy stored is only reduced by 13%. In the discharging mode, the process duration is reduced from 25 min to 9 min by increasing the heat transfer fluid (HTF) flow rate from 50 L·h^{−1} to 150 L·h^{−1}. In the direct heat transfer mode, the energy stored in the PCM depends on both the cooling power and the HTF flow rate, and can vary from 220 kJ for a cooling power at 30% and HTF flow rate of 50 L·h^{−1} to 4 kJ for a compressor power at 15% and a HTF flow rate of 150 L·h^{−1}. The novel heat exchanger is a feasible solution to implement latent energy storage in vapour compression systems resulting to a compact and less complex system.

Keywords: heat exchangers; thermal energy storage (TES); phase change materials (PCMs); refrigeration cycle; cooling applications; experimental study

1. Introduction

According to the International Institute of Refrigeration, the total number of refrigeration, air-conditioning, and heat pump systems worldwide in operation is about three billion, which accounts for about 17% of overall electricity consumption worldwide [1]. This share is expected to increase due to increasing life standards and cooling demand in numerous fields. As a consequence, this will pose more threats on climate change [2–4], especially because fossil fuels are the major primary sources of electricity production [3,5]. Conversely, the primary energy consumption as well as greenhouse gas (GHG) emissions can be reduced by using higher efficiency components and/or renewable energy sources coupled with thermal energy storage (TES) modules.

Usually, cooling systems are mainly categorized into refrigeration and air-conditioning systems, and are widely used in both industrial and domestic applications [6]. Refrigeration systems are mainly used for maintaining products at low temperature, while air-conditioning systems are used for controlling and regulating temperature and humidity of a closed environment. The performances of

refrigeration and air-conditioning systems based on a vapour compression cycle highly depend on their main components and boundary conditions, i.e., compressor, heat exchangers (evaporator and condenser), insulation, refrigerant type, thermal loads, and ambient conditions. In fact, the modification of the compressor, refrigerant, and insulation is a great challenge due to economic, environmental, and technological reasons, thus leading to more interest in the design and development of the condenser and the evaporator [7].

Additionally, the coefficient of performance of the refrigeration cycle (COP_R) is defined as, $COP_R = \frac{Q_1}{W_{in}}$, whereby Q₁ is the cooling capacity at the evaporator while W_{in} is the compressor work. Theoretically, the performance of the refrigeration cycle would be improved by raising the evaporator pressure achieving less power consumption by the compressor W_{in}, as shown in Figure 1a, and/or by increasing the sub-cooling degree, which would achieve higher cooling capacity Q₁, as shown in Figure 1b [8].

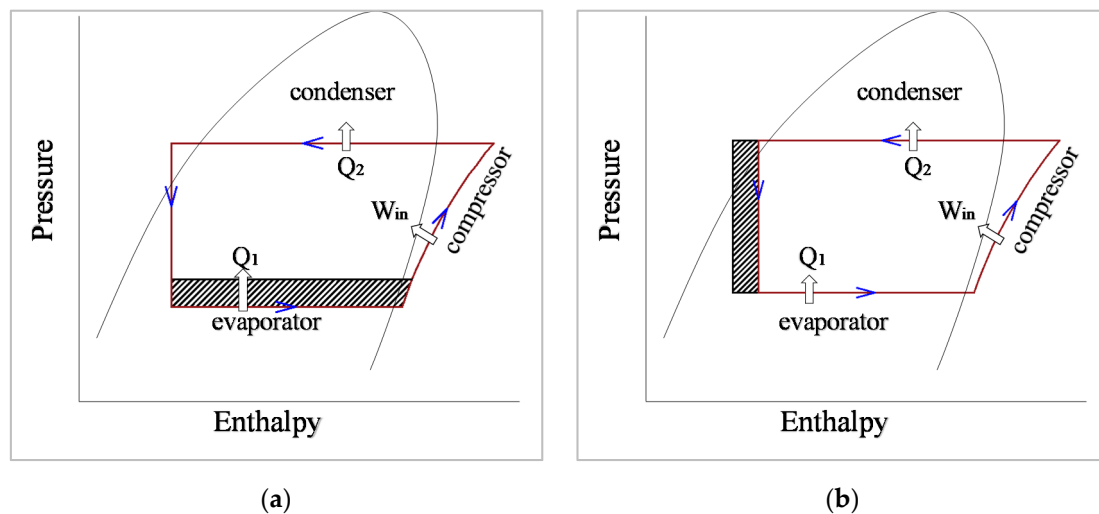


Figure 1. Pressure-enthalpy diagram of a refrigeration cycle with performance improvement by (a) raised evaporator pressure or (b) increased sub-cooling degree.

Correspondingly, thermal energy storage (TES) using phase change material (PCM) is a promising solution to achieve an increase of the sub-cooling degree, and/or an increase of the evaporation pressure, resulting to higher performance of the refrigeration/air-conditioning system. PCM has gained more interest due to its advantages over sensible heat storage, such as higher energy density and ability to absorb and release energy at constant temperature, hence requiring less space than using sensible energy storage [9–11].

The implementation of PCM into a refrigeration cycle has been investigated among researchers both in the internal and external part of the refrigerant circuit. For instance, Cheng et al. [12] experimentally investigated the PCM incorporation into a refrigeration cycle, by wrapping shape-stabilized PCM at the external tubes of the condenser. Unlike the basic system, heat dissipation was continuous even when the compressor went off, leading to higher sub-cooling degree, which consequently raised the coefficient of performance (COP) of the system. However, the frequency of the compressor ON/OFF also increased. Similarly, Wang et al. [13] performed an experimental investigation by placing a shell and tube PCM heat exchanger at different positions in the refrigeration cycle, and observed that, apart from an increased COP in all cases, when the PCM heat exchanger was placed between the evaporator and the compressor, a lower superheat and stable suction temperature was achieved. Cheng et al. [14] performed a numerical model which predicted that, by placing PCM at the evaporator leads to lower ON/OFF frequency of compressor than by placing PCM at the condenser, which is a desirable parameter for the compressor lifecycle. Azzouz et al. [15,16] numerically and experimentally investigated the influence of placing a PCM slab at the back side of the evaporator in a refrigerator and

reported the PCM to maintain the temperature for longer time in absence of power supply, leading to improved performance compared to the conventional systems. Copertaro et al. [17] placed a novel air heat exchanger, containing PCM that melts at 5 °C, near an evaporator inside a cold room, comparing the thermal behaviour with and without PCM, and reported maintenance of thermal conditions of the stored products, reduced number of ON/OFF cycles (six cycles by thirteen cycles) with PCM in the room. Despite of the abovementioned studies, the integration of PCM into the heat exchangers of refrigeration cycles is a topic not deeply investigated in the literature. Furthermore, previous attempts of PCM integration into refrigeration cycles involves introducing extra components, which would lead to complexity in assembling of the system, or a need for an extra space.

This study investigates for the first time a novel three-fluid refrigerant-PCM-water heat exchanger (RPW-HEX), all in a single component. The RPW-HEX was directly integrated into a vapour compression system, replacing the conventional evaporator, and it was connected to an external heat transfer fluid (HTF) loop, which simulates the heat source (thermal load).

This ALL-IN-ONE component provides double benefits, i.e., it works as a heat exchanger and as a TES module, and it is able to take advantage of the PCM high energy storage density and isothermal energy supply that would lead to peak shifting and peak shaving in the refrigeration cycle. Experiments were performed based on three modes. The first two modes treat the RPW-HEX as a TES tank, testing the charging and discharging of PCM. The third mode treats it as a heat exchanger medium among three fluids, which attests for ability to cover energy demand while storing extra cold energy, when the compressor is ON, and to release the stored cold energy when the compressor goes OFF. Finally, a parametric study is carried out on the influence of compressor power, evaporation temperature set-point, HTF inlet temperature and HTF flow rate on the RPW-HEX.

2. Methodology

2.1. Description of the Innovative Refrigerant-PCM-Water Heat Exchanger

In this paper, an innovative compact 3-fluids refrigerant-PCM-water heat exchanger (RPW-HEX) shown in Figure 2a is proposed, as a solution to reduce bulkiness and complexity of integration of latent heat TES into vapour compression systems, especially while assembling the final components. The RPW-HEX was designed and manufactured by AKG (Hofgeismar, Germany) and it contains 7 sections: the central part of the RPW-HEX (block A), one distributor for the HTF and one for the refrigerant (blocks W1 and R1), one collector for the HTF and one for the refrigerant (blocks W2 and R2), and two PCM storage containers (block P1 and P2) to provide space for expansion of the PCM. The main focus of the design of the RPW-HEX is the centre section (block A), which is designed to incorporate refrigerant, PCM, and HTF in an array of parallel channels integrated in a unique container, hence eliminating the need of having extra components (i.e., TES tank, HEX, valves, etc.) in the overall system. The channels are distributed in a regular way following the order of refrigerant—PCM—HTF, as shown in Figure 2b. This configuration allows simultaneous direct heat transfer between the refrigerant and both the HTF and the PCM. To enhance the heat transfer, the refrigerant and the HTF flow in counter-flow configuration.

The RPW-HEX is made of 600 °C dip-brazed 3000 aluminium core alloy, which provides high mechanical stability to withstand the volume expansion of the PCM and the refrigerant pressure inside the RPW-HEX. The low density of aluminium allows construction of relatively light structure of the RPW-HEX. Moreover, the high thermal conductivity and low cost of aluminium over other metals encourages even more its use in construction of the heat exchangers.

Table 1 presents the main structural characteristics of the RPW-HEX in study. The RPW-HEX external structural size is 300 mm × 272 mm × 94 mm, while internally it contains a total of 45 channels (15 PCM channels, 14 refrigerant channels, and 16 HTF channels). An extra channel of the HTF is designed to isolate the refrigerant channel from the external surface to lessen the possible cold losses to the ambient, thus both the top and the bottom of the tank contain the HTF channel. Fins are embedded

among the HTF, refrigerant, and PCM channels to enhance heat transfer. Each refrigerant and HTF channel contains 43 fins, while each PCM channel contains a total of 33 fins. The RPW-HEX channels containing the PCM are constructed of dense geometry of aluminium offset strip fins to increase heat transfer through the PCM taking advantage of the high thermal conductivity of aluminium.

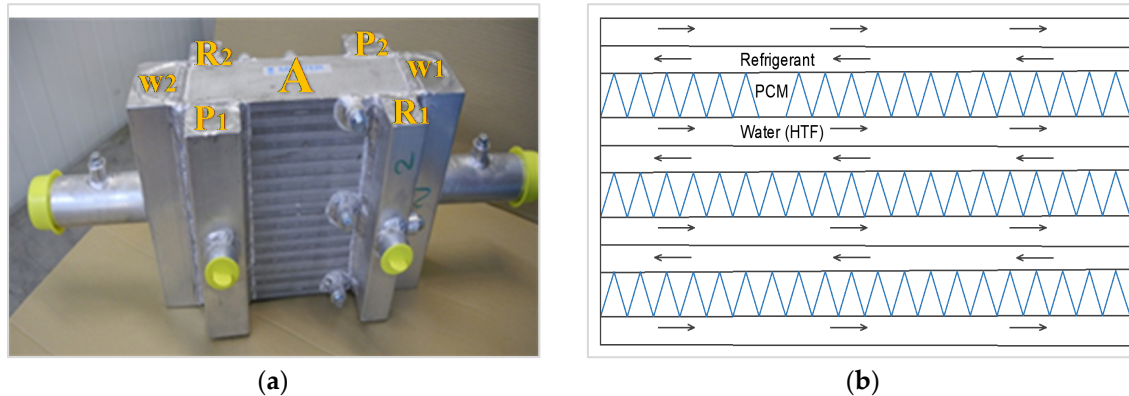


Figure 2. Innovative refrigerant-phase change material (PCM)-water heat exchanger (AKG, Germany): (a) external structure and (b) internal distribution of the channels.

Table 1. Main characteristics of the refrigerant-PCM-water heat exchanger (RPW-HEX).

Characteristic	Refrigerant	HTF	PCM
Number of channels [-]	14	16	15
Height of channels [mm]	3	3	10
Number of fins [-]	43	43	33
Volume of the fluid [L]	0.65	0.8	2.5
Core length × width × depth [mm]	300 × 272 × 94		

2.2. Experimental Setup

A dedicated experimental setup to test the innovative RPW-HEX (Figure 3) was built at the laboratory of the GREiA research group at the University of Lleida in Spain. The schematic of the experimental setup is shown in Figure 4, and it mainly consists of two fluid circuits: one refrigerant circuit and one HTF circuit. The refrigerant circuit includes the RPW-HEX (1) acting as the evaporator, a variable cooling capacity condensing unit (Zanotti model GCU2030ED01B) containing a hermetic scroll compressor (CU E scroll digital) in (2), and air-cooled condenser in (3), working with R449A refrigerant. An electronic expansion valve (4) is used to expand the liquid refrigerant coming from the condenser before it enters the RPW-HEX. According to the manufacturer, the condensing unit has a maximum cooling power of 4.956 kW and a COP of 2.12 when working under ambient temperature of 32 °C with fixed evaporation temperature of −10 °C.

The HTF circuit consists of a water bath (5) containing a pump (6) to circulate the HTF, $\frac{1}{2}$ " copper pipes, valves (7) and (8) to control the flow, and an advanced volumetric flow meter (Badger Meter Primo) (9) with an accuracy of $\pm 0.25\%$ to measure the flow rate of the HTF. To obtain a stable HTF temperature at the RPW-HEX inlet, the water bath is embedded with an internal electric heater (10) and is supplemented with two chillers (JP SELECTA FRIGEDOR-285W) (11) and two immersion heaters (OVAN TH100E-2kW and JP SELECTA-1kW) (12).

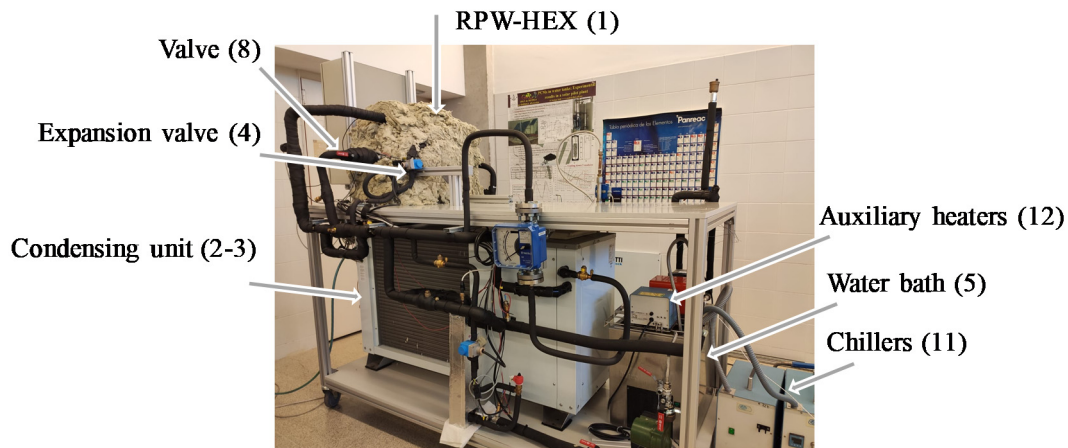


Figure 3. Experimental setup of the innovative refrigerant-PCM-water heat exchanger integrated into a simple vapour compression system.

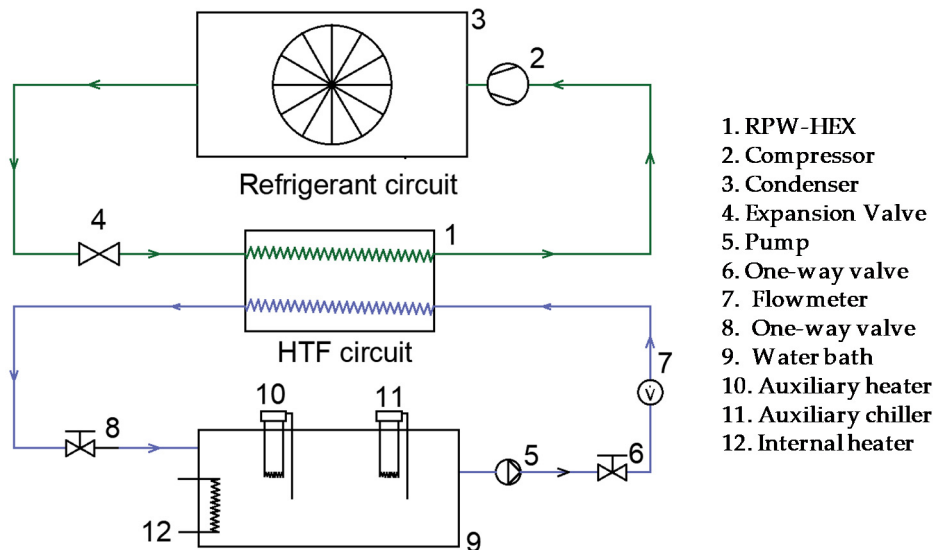


Figure 4. Schematic diagram of the experimental setup showing heat transfer fluid (HTF) circuit and the refrigerant circuit.

The innovative RPW-HEX (1) is connected to both the refrigerant circuit and the HTF circuit. During the tests, the RPW-HEX was well insulated with 12-cm thick rock wool material to reduce heat losses to the ambient air to an extent such that one can assume heat exchange only among HTF, PCM, and the refrigerant.

For system monitoring and data acquisition, a total of 13 temperature sensors (Pt-100 class B, IEC 60751 standard type) with uncertainty of ± 0.3 °C were distributed within the RPW-HEX. Nine sensors were placed in contact to the PCM, while for each inlet and exit of the RPW-HEX a temperature sensor was positioned to measure the temperature of the HTF and the refrigerant (Figure 5). The sensors were connected to a data acquisition system (STEP DL-01 data logger) connected to a computer with Indusoft SCADA software to record the experimental measurements every 10 s.

2.3. Materials and Properties

An amount of 3.15 kg of the commercial RT4 PCM provided by Rubitherm company [18] was embedded into the RPW-HEX for latent thermal energy storage. The RT4 is an organic (paraffin) PCM thermally stable and chemically inert. The thermo-physical properties as provided by the manufacturer are provided in the Table 2.

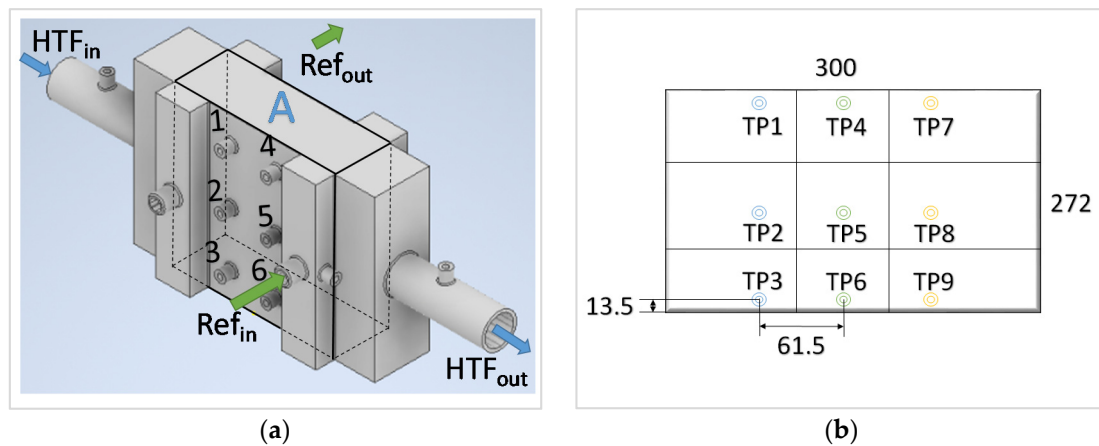


Figure 5. Position of the sensors in the refrigerant-PCM-water heat exchanger: (a) all sensors and (b) only PCM sensors.

Table 2. Properties of the commercial RT4 PCM [18].

Properties	Value	Units
Phase change range	2–4	°C
Density	0.88 (solid) 0.77 (liquid)	kg·L ^{−1}
Thermal conductivity	0.2	W·m ^{−1} ·K ^{−1}
Volume expansion	12.5	%

To determine the specific enthalpy of the PCM, DSC 3+ Mettler Toledo equipment with ± 0.2 K accuracy available in GREiA research group at university of Lleida was used [19]. From the results shown in Figure 6 the phase change temperature was found to be around 5 °C.

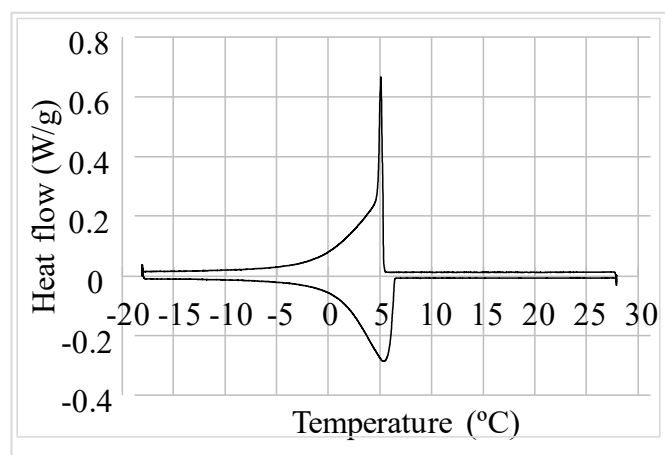


Figure 6. DSC results of heat flow in charging and discharging of the commercial PCM RT4 (adapted from [19]).

Water-glycol mixture with a concentration of 70% water by 30% glycol was used as the HTF. Table 3 presents the thermo-physical properties of the HTF as given by the manufacturer [20].

Table 3. HTF (water-glycol) properties at different temperatures.

Properties	At T = −4 °C	At T = 12 °C	Units
Density	1053.5	1047.4	kg·m ^{−3}
Viscosity	4.8	2.8	mPa·s
Specific heat	3579	3624	J·kg ^{−1} ·K ^{−1}
Conductivity	0.418	0.437	W·m ^{−1} ·K ^{−1}
Freezing Temperature	−18		°C
Boiling temperature	127		°C

2.4. Experimental Methodology

The experiments were performed in different operating modes: Mode 1—charging, Mode 2—discharging, and Mode 3—simultaneous charging and discharging of the RPW-HEX. The experiment is considered in charging mode when the refrigerant circuit provides cold to the RPW-HEX in the condition when the HTF is not flowing through the RPW-HEX, while it is considered in discharging mode when the RPW-HEX provides cold to the HTF circuit in the condition when the refrigerant circuit is switched off. In either Mode 1 or Mode 2, only one circuit is switched on during each experimental test, while in Mode 3 both the refrigerant and HTF circuits are open allowing heat exchange among the latter two and the PCM in the RPW-HEX. For each of the three modes, different working conditions were tested. Before starting any experiment, the PCM, water bath, and the condensing unit were set to the required experimental conditions. At least three repetitions were performed in each mode to check the repeatability and robustness of the results.

2.4.1. Mode 1: Charging

In all the charging test, the RPW-HEX was initially completely discharged by setting the PCM temperature to 12 ± 0.5 °C. This value was selected because it is the most common temperature of the return water of refrigeration systems in buildings. Charging tests were started by switching on the condensing unit after preparing the initial experimental conditions. Several experiments were performed at different values of the cooling power (%) of the condensing unit, as shown in Table 4. Each experiment was considered complete when the condensing unit automatically switched off because the evaporation temperature reached the set-point value (−10 °C).

Table 4. Set of experiments in Mode 1.

Initial PCM Temperature [°C]	Compressor Power [%]	Evaporation Set-Point [°C]
12	15	−10
	30	
	45	
	60	
	75	

Additionally, −18 °C was also used as evaporation temperature set-point of the condensing unit at 15% cooling power to investigate the effect of this parameter on the RPW-HEX charging process. The value of −10 °C was chosen as it is the value recommended by the manufacturer's datasheet, and for which the condensing unit was optimized, while the value of −18 °C temperature was selected taking into account that lower than that would lead to freezing of the HTF inside the RPW-HEX, which could irreversibly damage it. The condensing unit stopped whenever the set-point temperature was achieved.

2.4.2. Mode 2: Discharging

In all discharging experiments, the RPW-HEX was initially charged, which was achieved by setting the PCM temperature to $-4\text{ }^{\circ}\text{C}$. This value was chosen as the level of complete charge because it was the temperature at which a satisfactory uniform temperature distribution was achieved in the PCM after most of the charging processes for which the evaporation set-point was $-10\text{ }^{\circ}\text{C}$. The partial enthalpy between $-4\text{ }^{\circ}\text{C}$ and $12\text{ }^{\circ}\text{C}$ represents around 90% of the total enthalpy of the PCM in the maximum temperature range that extends between the minimum ($-10\text{ }^{\circ}\text{C}$) and the maximum ($12\text{ }^{\circ}\text{C}$) possible temperatures. The experiments were started when all the sensors were below $-4\text{ }^{\circ}\text{C}$ to ensure that the RPW-HEX was completely charged. The HTF circuit was opened and the inlet HTF temperature was maintained constant. The experiments were performed at $50\text{ L}\cdot\text{h}^{-1}$, $100\text{ L}\cdot\text{h}^{-1}$, and $150\text{ L}\cdot\text{h}^{-1}$ HTF flow rate, and at different HTF inlet temperatures of $9\text{ }^{\circ}\text{C}$, $12\text{ }^{\circ}\text{C}$, and $15\text{ }^{\circ}\text{C}$, as shown in Table 5. The discharging process was considered completed when the difference between the HTF temperature at the inlet and outlet of the RPW-HEX were at most $0.5\text{ }^{\circ}\text{C}$.

Table 5. Set of experiments in Mode 2.

Initial PCM Temperature [$^{\circ}\text{C}$]	HTF Inlet Temperature [$^{\circ}\text{C}$]	HTF Flow Rate [$\text{L}\cdot\text{h}^{-1}$]
−4	09	150
	12	
	15	
−4	09	100
	12	
	15	
−4	09	50
	12	
	15	

2.4.3. Mode 3: Simultaneous Charging and Discharging

The experiments in Mode 3 were performed when both the HTF and refrigerant circuits were switched on, hence allowing direct heat exchange between the condensing unit and the water bath through the RPW-HEX. Two types of experiments were performed in this mode, depending on the initial state of the RPW-HEX. That is, for the first case the RPW-HEX was initially completely discharged while for the second case it was initially completely charged.

In Mode 3a, the PCM was initially at $12\text{ }^{\circ}\text{C}$, which is the temperature at which the RPW-HEX is considered totally discharged. The HTF flow rate was set to either $50\text{ L}\cdot\text{h}^{-1}$, $100\text{ L}\cdot\text{h}^{-1}$ or $150\text{ L}\cdot\text{h}^{-1}$, while the water bath temperature was maintained at $12\text{ }^{\circ}\text{C}$, which is the typical HTF temperature at evaporator inlet in cooling applications in buildings. When all the sensors within the RPW-HEX were at $12 \pm 0.5\text{ }^{\circ}\text{C}$, the condensing unit and the HTF pump were switched on to initiate the experiment. The experimental plan in Mode 3a is shown in Table 6.

Table 6. Set of experiments in Mode 3a.

Initial PCM Temperature [°C]	Compressor Power [%]	Evaporation Set-Point Temperature [°C]	Inlet HTF Temperature [°C]	HTF Flow Rate [L·h ⁻¹]
12	15	−10	12	150
	30			
	45			
	60			
	75			
12	15	−10	12	100
	30			
	45			
	60			
	75			
12	15	−10	12	50
	30			
	45			
	60			
	75			

The experiments in Mode 3b are similar to those in Mode 3a with the exception that the initial temperature of the PCM was set at −4 °C, at which the RPW-HEX is considered completely charged. The experimental plan in Mode 3b is shown in Table 7.

Table 7. Set of experiments in Mode 3b.

Initial PCM Temperature [°C]	Compressor Power [%]	Evaporation Set-Point Temperature [°C]	Inlet HTF Temperature [°C]	HTF Flow Rate [L·h ⁻¹]
−4	15	−10	12	150
	30			
	45			
	60			
	75			
−4	15	−10	12	100
	30			
	45			
	60			
	75			
−4	15	−10	12	50
	30			
	45			
	60			
	75			

2.5. Theoretical Evaluation Methodology

In order to analyse and compare the charging and discharging of the PCM in the different modes, nine well distributed temperature sensors were used, thus dividing the container into nine respective sections, as shown in Figure 5. The amount of PCM at each section was evaluated as shown in Equation (1):

$$m_i = \frac{l_i \cdot w_i}{l \cdot w} \cdot \rho_l \cdot v_T [\text{kg}] \quad (1)$$

where l_i and w_i are the length and the width of PCM section “i”, l and w are the length and the width of the region occupied by PCM (Block A), v_T is the total volume of PCM inside the tank that is in direct

thermal contact with the refrigerant and HTF channels, and ρ_l is the density of PCM in liquid state. It is assumed that the mass of PCM inside each section of the PCM remains constant regardless the state of the PCM during the phase change process.

The specific enthalpy of the PCM was derived from DSC results shown in Figure 6 to relate the cold energy stored in the PCM with its temperature, as shown in Equation (2):

$$\begin{cases} h_i = h_{T_{-4^\circ\text{C}}} + C_{p_s}(-4 - T_i) \left[\text{kJ}\cdot\text{kg}^{-1} \right], & \text{if } T_i < -4^\circ\text{C} \\ h_i = -0.1139 \cdot T_i^3 + 1.1139 \cdot T_i^2 - 8.5545 \cdot T_i + 131.97 \left[\text{kJ}\cdot\text{kg}^{-1} \right], & \text{if } -4^\circ\text{C} \leq T_i < 6^\circ\text{C} \\ h_i = -0.0985 \cdot T_i^3 + 2.8732 \cdot T_i^2 - 28.629 \cdot T_i + 99.839 \left[\text{kJ}\cdot\text{kg}^{-1} \right], & \text{if } 6^\circ\text{C} \leq T_i \leq 12^\circ\text{C} \\ h_i = -C_{p_l}(T_i - 12) \left[\text{kJ}\cdot\text{kg}^{-1} \right], & \text{if } T_i > 12^\circ\text{C} \end{cases} \quad (2)$$

where h_i and T_i are the specific enthalpy and instantaneous temperature of the PCM at section “i”, respectively. The specific heat capacity values of the PCM at temperatures less than -4°C and higher than 12°C were considered constant and equal to $C_{p_s} = 2.03 \text{ kJ}\cdot\text{kg}^{-1}\cdot\text{K}^{-1}$ and $C_{p_l} = 1.10 \text{ kJ}\cdot\text{kg}^{-1}\cdot\text{K}^{-1}$, respectively.

The total cold energy stored in the PCM ($E_T(t)$) and the power of charging or discharging of the cold energy ($\dot{E}_T(t)$) at a given time t were evaluated as described in Equations (3) and (4), respectively:

$$E_T(t) = \sum_{i=1}^9 m_i \cdot h_i(t) \text{ [kJ]} \quad (3)$$

$$\dot{E}_T(t) = \frac{dE_T(t)}{dt} \text{ [kW]} \quad (4)$$

3. Results

A summary of the results is presented below showing the temperature profiles in the PCM and the cold energy stored in the PCM under different operating conditions and modes. The nine temperature sensors distributed throughout the PCM as shown in Figure 5 are presented hereby as dotted lines at top level, i.e., from left to right TP1, TP4, and TP7, as dashed lines at the middle level, i.e., TP2, TP5, and TP8, and as solid lines at the bottom, i.e., TP3, TP6, and TP9. In the results presented, TR(IN) and TR(OUT) are the inlet and outlet refrigerant temperatures, respectively, while TW(IN) and TW(OUT) are the inlet and outlet HTF temperatures, respectively.

3.1. Mode 1: Charging

3.1.1. Temperature Profiles during the Charging of the PCM

In Mode 1, the influence of compressor power was evaluated using different compressor power as shown in Table 4. Figure 7 shows the PCM and refrigerant temperature evolution along time for compressor power at 30%, 45%, and 60% respectively. It was observed that the PCM at the top of the RPW-HEX was not fully charged (i.e., it was not completely solidified), while the middle and the bottom levels were completely charged resulting to temperature around -10°C . In addition, it was observed that the time for charging process to be completed (i.e., the condensing unit to switch off) was 17 min, 7.5 min, and 6.5 min for compressor power at 30%, 45%, and 60% respectively.

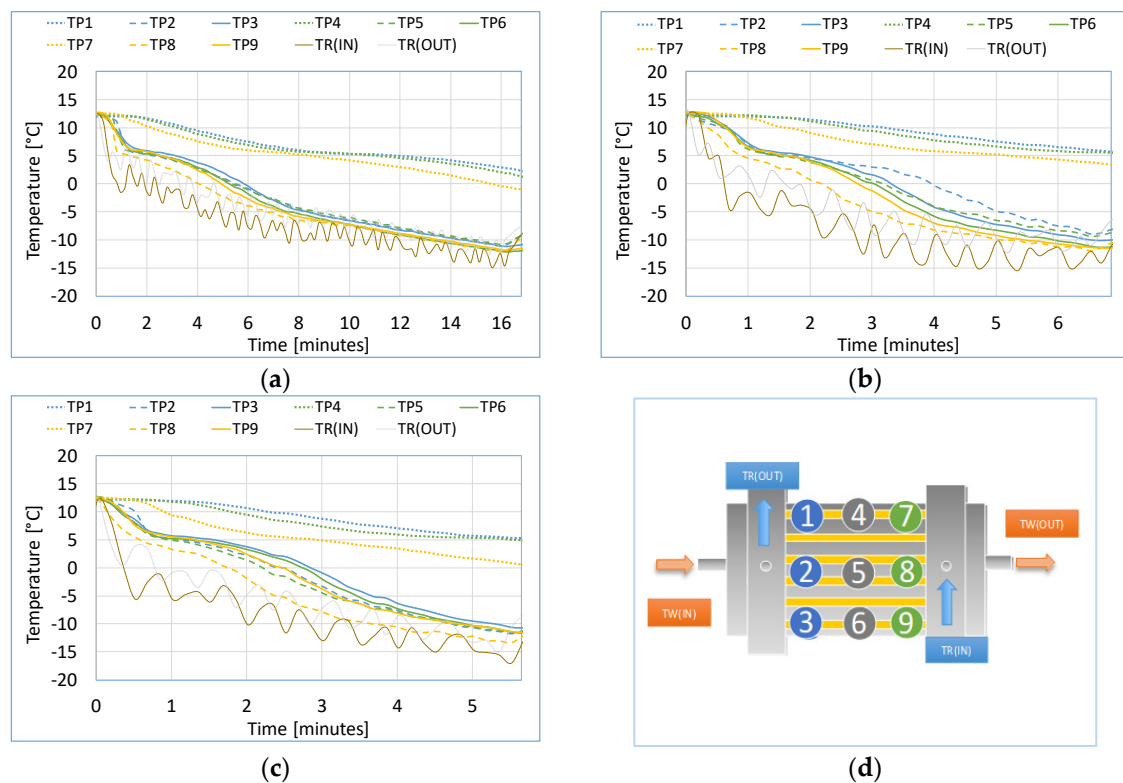


Figure 7. Temperature profiles in Mode 1 for compressor power at (a) 30%, (b) 45%, (c) 60% and (d) position of the sensors. Dotted lines denote PCM temperature at top level, dashed lines at middle level, and solid lines at the bottom.

As shown in Figure 7, the PCM located at the middle and bottom of the RPW-HEX start to solidify after around 1 min from the beginning of the experiments, while the PCM located at the top requires much more time to start the solidifying process. This means that the charging of the PCM is not uniform, and if the charging duration is not long enough, there are zones of the RPW-HEX where the PCM is not completely solidified. Although increasing the compressor power accelerates the solidification at the top region, it is not able to completely solidify since the charging process stops earlier because the evaporation temperature reaches the set-point.

Another possibility was investigated to find out if it was possible to reach a complete PCM solidification in the entire RPW-HEX. To do this, the evaporation temperature was decreased down to the security set-point given by the freezing point of the HTF, i.e., $-18\text{ }^{\circ}\text{C}$. As shown in Figure 8, by decreasing the compressor set-point, and for a low compression power (15%), the PCM was completely solidified after 50 min. Furthermore, the temperature distribution inside the PCM became more uniform over time, and a maximum temperature difference below $2\text{ }^{\circ}\text{C}$ was achieved after 300 min, when the compressor switched off because it reached the security set-point. However, despite that fact that the RPW-HEX was completely charged and a uniform temperature distribution inside the PCM was achieved, this strategy has some major drawbacks, such as a very long charging process duration, and a decrease of the energy efficiency of the condensing unit.

3.1.2. Cold Energy Stored, Energy Storage Rate and Time Required to Charge the PCM

Figure 9 shows the PCM instantaneous cold energy and the PCM energy storage rate against time during the charging test with a compressor power 30%. It was observed that from the second to the fifth minute the energy storage rate is quite higher than in the rest of the process. This is explained by the fact that most of the PCM is changing phase during this period, allowing for a higher temperature difference between the refrigerant and the PCM.

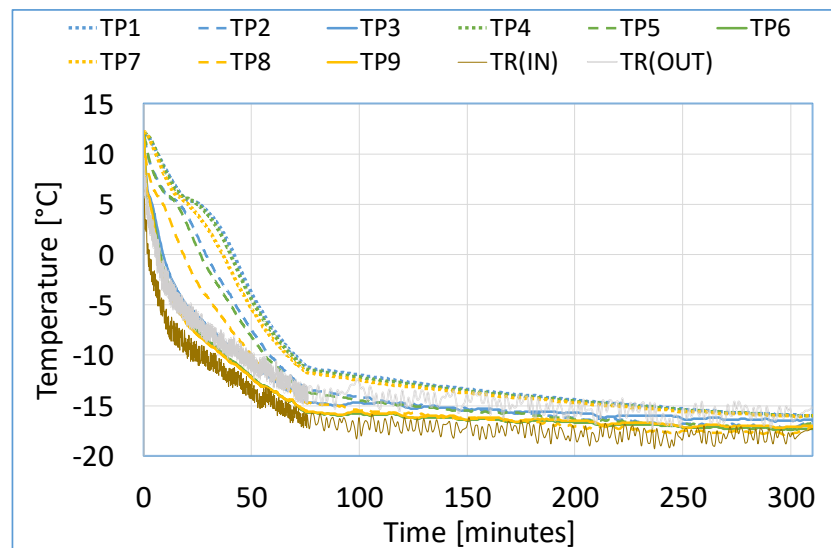


Figure 8. PCM temperature profile for compressor power at 15% in Mode 1. Dotted lines denote PCM temperature at top level, dashed lines at middle level, and solid lines at the bottom.

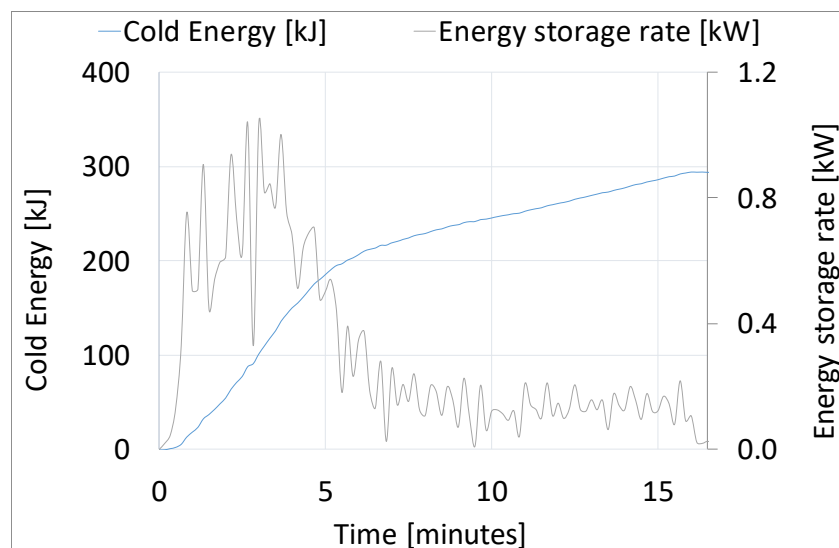


Figure 9. Cold energy and energy storage rate against time, for PCM charging at 30% compressor power.

The final cold energy stored in the PCM and charging time are reported in Figure 10 for the different compressor powers investigated to evaluate the influence of compressor power on the total cold energy that can be stored. It was observed that the lower the compressor power the higher the time of charging. Moreover, the highest energy storage capacity was achieved at a compressor power of 30%, for which 294 kJ of cold energy were stored in 17 min. The second higher value of cold energy stored in the PCM was achieved at a compressor power of 60%, for which 273 kJ of cold energy were stored in 6.7 min. This represents a decrease of about 7% in the energy stored, but the charging duration was considerably reduced from 17 min to less than 7 min, which represents a reduction of about 60%. Therefore, if the charging duration is a critical parameter of the real application, the charging at 60% compressor power could be a good option.

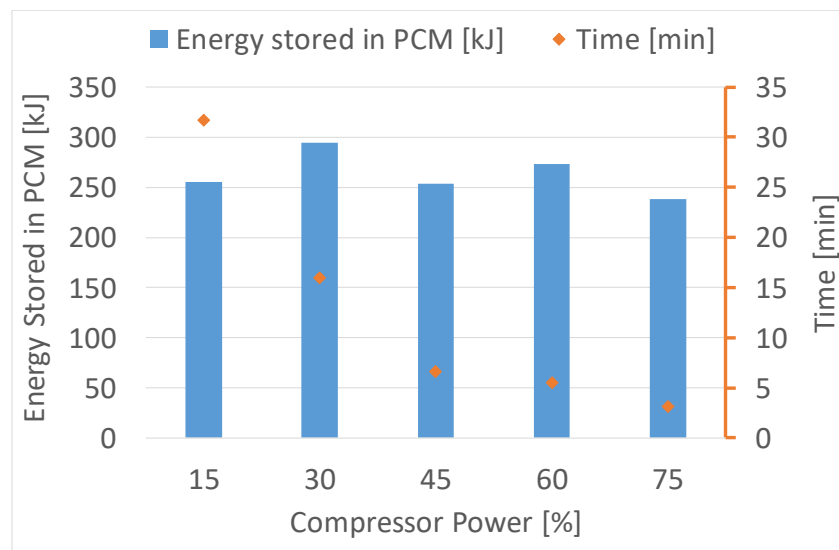


Figure 10. Influence of compressor power on total cold energy stored in the PCM.

3.2. Mode 2: Discharging

3.2.1. Temperature Profiles during the Discharging of the PCM

Regarding Mode 2, the influence of both HTF inlet temperature and flow rate was evaluated with the PCM initially at $-4\text{ }^{\circ}\text{C}$. Figure 11 shows the PCM and HTF temperature profiles in Mode 2 for HTF inlet temperature at $9\text{ }^{\circ}\text{C}$, $12\text{ }^{\circ}\text{C}$, and $15\text{ }^{\circ}\text{C}$, and at constant HTF flow rate of $100\text{ L}\cdot\text{h}^{-1}$. It was observed that the PCM discharging time is shortest for the highest inlet temperature, because of the higher temperature difference between the PCM and the HTF that increases the heat transfer rate.

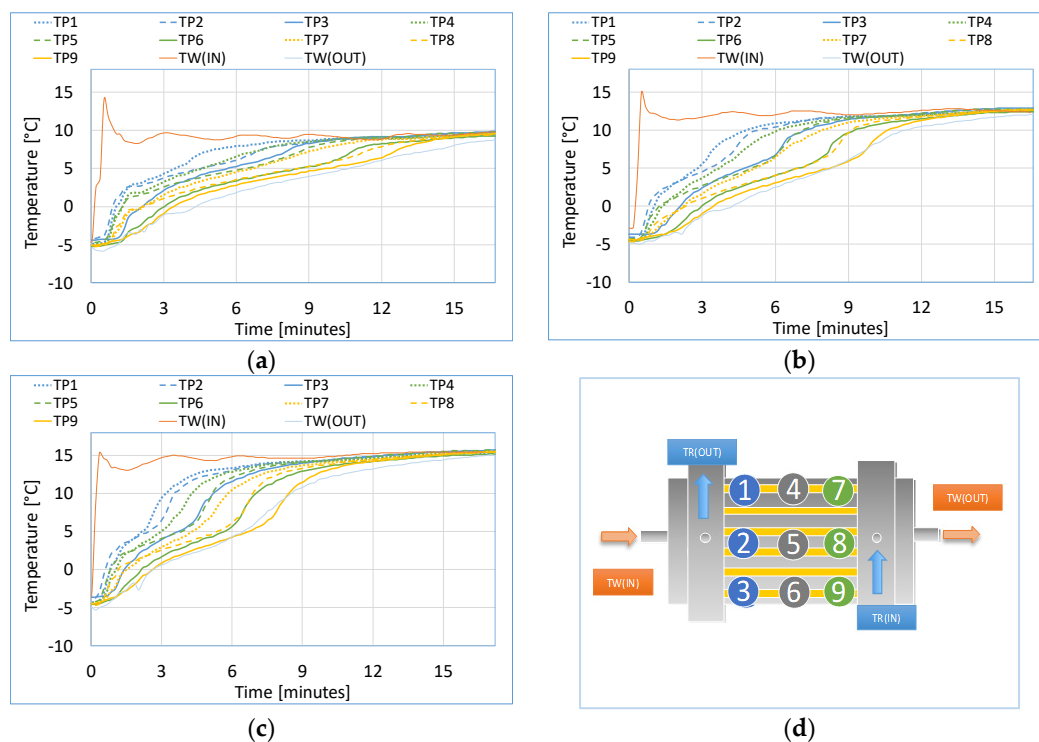


Figure 11. PCM temperature profile during discharging at $100\text{ L}\cdot\text{h}^{-1}$ with HTF inlet temperature at (a) $9\text{ }^{\circ}\text{C}$, (b) $12\text{ }^{\circ}\text{C}$, and (c) $15\text{ }^{\circ}\text{C}$ and (d) position of the sensors. Dotted lines denote PCM temperature at top level, dashed lines at middle level, and solid lines at the bottom.

A temperature gradient was observed inside the PCM in the direction parallel to the HTF flow (see the curves of the same colour presenting temperature profiles) since the HTF is cooling down as it flows through the RPW-HEX by releasing heat to the PCM, which causes the phase change front to progressively move in the direction from the HTF inlet towards the outlet. However, a temperature gradient is also observed from the top to the bottom of the PCM tank, being the PCM temperature at the top part of the RPW-HEX higher than at the bottom (see the curves of the same type). This means that the HTF stratifies inside the tank, which causes an asymmetric PCM melting that starts earlier at the top part. During PCM phase change, the temperature difference between the top and the bottom of the tank is around 3 °C at all locations and for all HTF inlet temperatures tested.

Figure 12 shows the PCM and HTF temperature profiles in Mode 2 for HTF inlet temperature of 12 °C and flow rates of 50 L·h⁻¹, 100 L·h⁻¹, and 150 L·h⁻¹, respectively. Hereby, the duration of the discharging process decreases by increasing the HTF flow rate. At the lowest flow rate value, the melting front requires around 15 min to move from one edge of the tank to the opposite one, while for the highest flow rate value it requires around 4 min. Both the stratification of the HTF inside the RPW-HEX, as well as the temperature gradient inside the PCM in the direction of HTF flow, are slightly reduced by increasing the HTF flow rate.

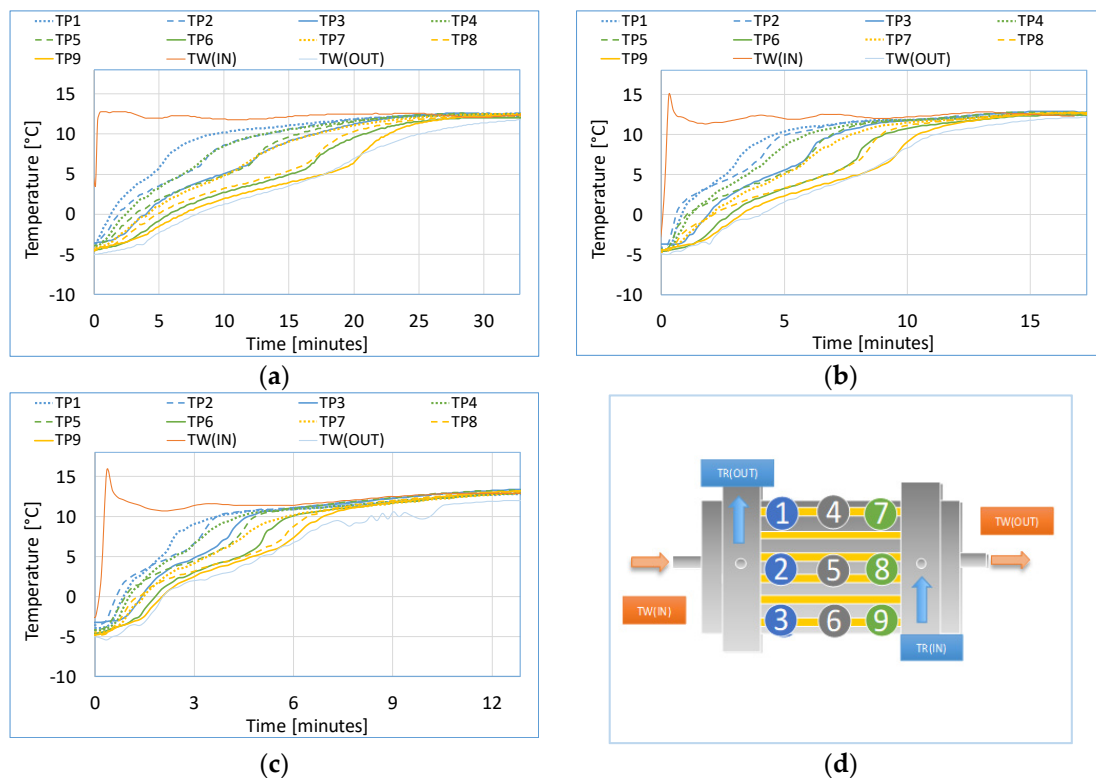


Figure 12. PCM temperature profile during discharging with HTF inlet temperature at 12 °C and at a flow rate of (a) 50 L·h⁻¹, (b) 100 L·h⁻¹, (c) 150 L·h⁻¹ and (d) position of the sensors. Dotted lines denote PCM temperature at top level, dashed lines at middle level, and solid lines at the bottom.

3.2.2. Instantaneous Cold Energy in PCM, Average PCM Discharge Rate and Time Required to Discharge the PCM

Figure 13 shows the influence of HTF inlet temperature on the PCM instantaneous cold energy at constant HTF flow rate of 100 L·h⁻¹. In the previous section it was observed that PCM can be completely discharged by HTF inlet temperature at either 12 °C or 15 °C, while it is only partially discharged at 9 °C. Considering that the PCM is completely discharged when the final temperature of 12 °C is achieved, the cold energy stored in the PCM can even take negative values when the HTF

temperature inlet is at 15 °C. Since the RPW-HEX was considered completely discharged at 12 °C, the negative values mean that it is over discharged beyond the limit.

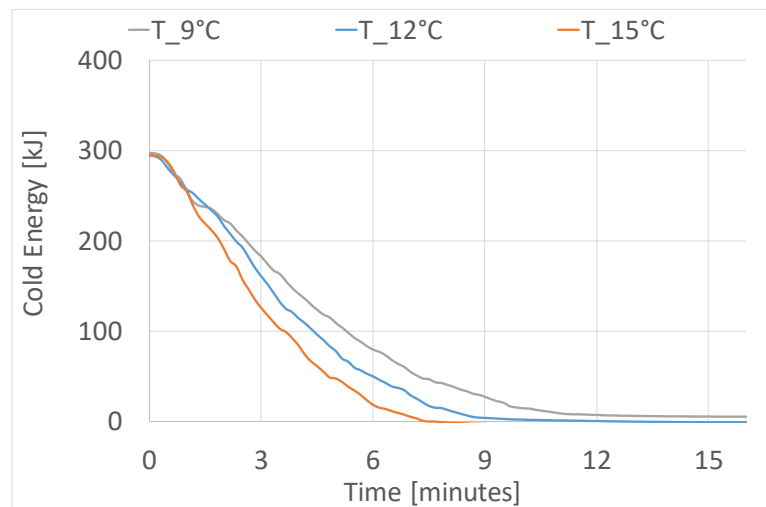


Figure 13. Influence of HTF inlet temperature on PCM instantaneous cold energy during discharging at constant HTF flow rate of 100 L·h⁻¹.

Figure 14 shows the influence of HTF inlet temperature on the average PCM discharge rate and time taken during the discharging mode at constant HTF flow rate of 100 L·h⁻¹. It is observed that at higher temperature values the PCM discharges faster than at low temperature values. In this case, it takes 8 min, 10 min, and 16 min for the HTF inlet temperature at 15 °C, 12 °C, and 9 °C, respectively, to discharge the cold energy stored in the PCM.

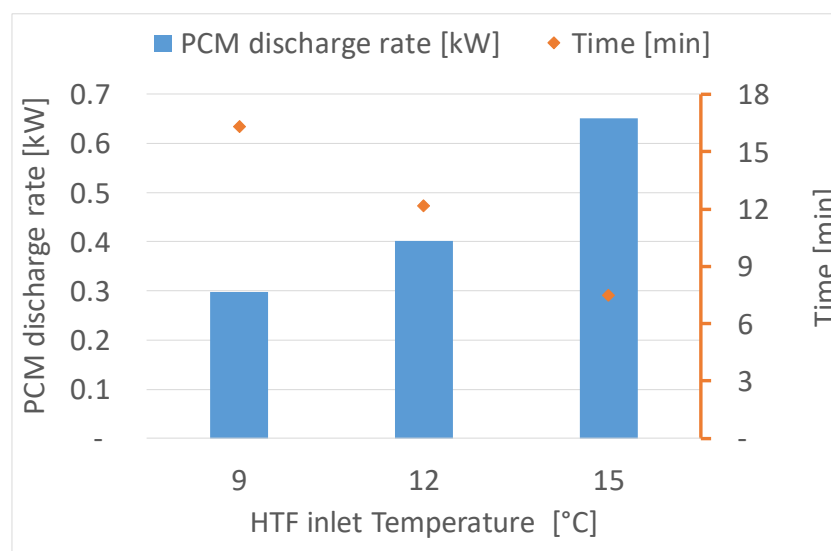


Figure 14. Influence of HTF inlet temperature on PCM discharge rate and time to complete discharging process at constant HTF flow rate of 100 L·h⁻¹.

Figures 15 and 16 show the influence of HTF flow rate on the instantaneous PCM cold energy, and the average PCM discharge rate and time taken during the discharging mode, respectively, at constant HTF inlet temperature of 12 °C. Hereby it is observed that the discharging time decreases with increasing HTF flow rate. It takes 9 min, 12 min, and 25 min to completely discharge the PCM with a HTF flow rate of 150 L·h⁻¹, 100 L·h⁻¹, and 50 L·h⁻¹, respectively.

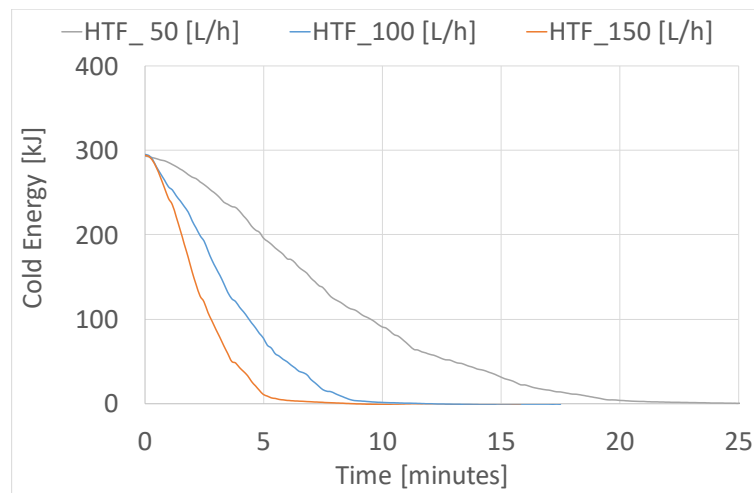


Figure 15. Influence of the HTF flow rate on the cold energy stored in the PCM during discharging at constant HTF inlet temperature of 12 °C.

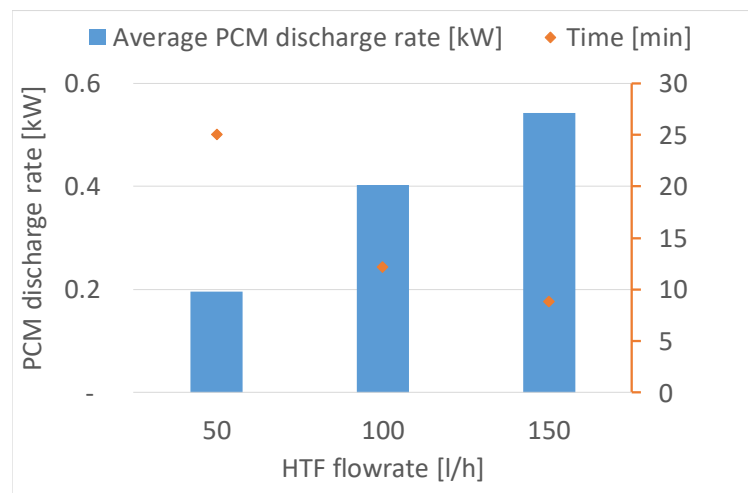


Figure 16. Influence of the HTF flow rate on the average PCM discharge rate and time of discharging at constant HTF inlet temperature of 12 °C.

3.3. Mode 3: Simultaneous Charging and Discharging

According to the set of experiments shown earlier in the methodology section, the experiments in Mode 1 and Mode 2 showed total feasibility, while for Mode 3a and 3b could only be performed partially because the condensing unit stopped in less than three minutes therefore not providing enough data to analyse. A summary of the feasibility of the experiments in Mode 3a and 3b is available in Tables 8 and 9, respectively.

Table 8. Feasibility of the set of experiments in Mode 3a.

Mode 3a: Initial Temperature at 12 °C			
Compressor Power [%]	Flow Rate [L·h ⁻¹]		
	50	100	150
15	✓	✓	✓
30	✓	✓	✓
45	X	✓	✓
60	X	✓	✓
75	X	X	X

Table 9. Feasibility of the set of experiments in Mode 3b.

Mode 3b: Initial Temperature at $-4\text{ }^{\circ}\text{C}$			
Compressor Power [%]	Flow Rate [$\text{L}\cdot\text{h}^{-1}$]		
	50	100	150
15	✓	✓	✓
30	X	X	X
45	X	X	X
60	X	X	X
75	X	X	X

3.3.1. Mode 3a: Simultaneous Charging and Discharging of the RPW-HEX with the PCM Initially Completely Discharged

Temperature Profiles during the Simultaneous Charging and Discharging of the PCM

In Mode 3a, both the refrigerant circuit and HTF circuit were simultaneously switched on, with the PCM initially at $12\text{ }^{\circ}\text{C}$. Figure 17 shows the temperature profile in Mode 3a for the experiments performed at an HTF flow rate of $100\text{ L}\cdot\text{h}^{-1}$ and inlet temperature of $12\text{ }^{\circ}\text{C}$, and for compressor powers at 30%, 45%, and 60%. In all the cases it was observed that, after a certain period of time, the RPW-HEX attained stable conditions, meaning that the cooling capacity of the refrigerant was entirely used to cool down the HTF, while the PCM remained at a constant temperature. Therefore, in steady state conditions the RPW-HEX does not act as an active energy storage component, but only as a heat exchanger. Furthermore, in steady state, the phase change was not fully achieved in all the PCM, especially at the top and near the HTF inlet (TP1 and TP4), meaning that the RPW-HEX was only partially charged. There is a strong temperature gradient inside the PCM in the vertical direction even at lower compressor powers, being the PCM temperature difference between the top and the bottom levels as high as $20\text{ }^{\circ}\text{C}$, at compressor power of 60%. This means that the region where most of the heat transfer takes place is towards the bottom part of the RPW-HEX probably because of a higher concentration of the liquid phase of refrigerant in that part due to its higher density, while the vapour phase of the refrigerant flows mainly on the top part without producing relevant cooling effect.

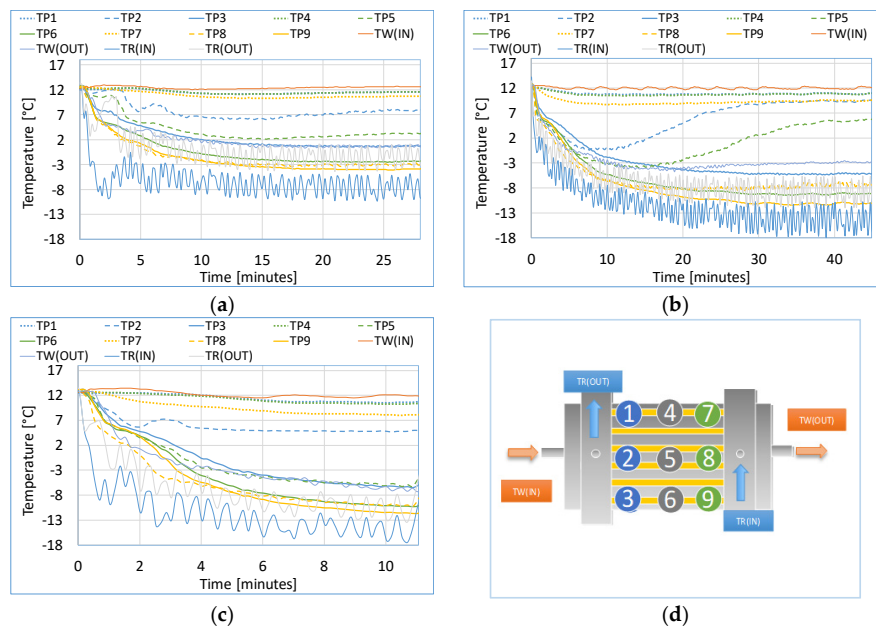


Figure 17. PCM temperature profile in Mode 3a with HTF inlet temperature at $12\text{ }^{\circ}\text{C}$ and at a flow rate of $100\text{ L}\cdot\text{h}^{-1}$, for compressor power of (a) 30%, (b) 45%, (c) 60% and (d) position of the sensors. Dotted lines denote PCM temperature at top level, dashed lines at middle level, and solid lines at the bottom.

Instantaneous Cold Energy in PCM, Total Cold Energy Storage and Time to Reach Equilibrium

Figure 18 shows the influence of compressor power on the PCM instantaneous cold energy. In this mode, part of the cooling capacity of the refrigerant is initially used to charge the PCM until steady state conditions are reached, and the RPW-HEX acts as a cold energy storage component. It is observed that the slope of the instantaneous cold energy curve is higher for higher compressor powers during the transient part of the process. When steady state conditions are achieved, the value of the cold energy remains constant. However, at compressor power of 60%, the evaporation temperature reaches at the set-point ($-10\text{ }^{\circ}\text{C}$) before thermal equilibrium was achieved.

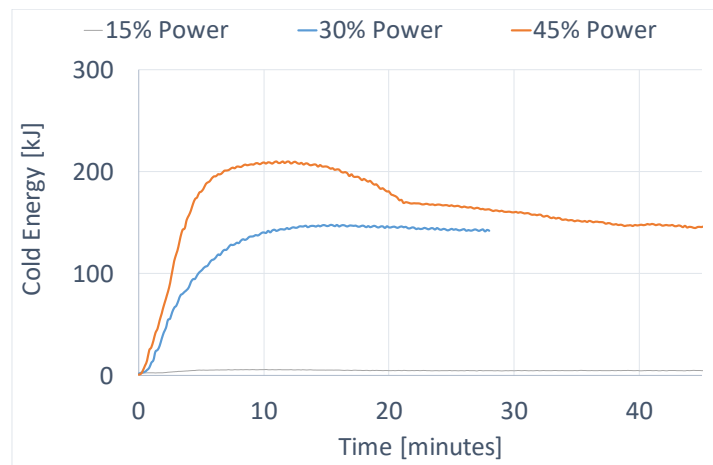


Figure 18. Influence of compressor power on the instantaneous cold energy stored in the PCM in Mode 3a with HTF inlet temperature at $12\text{ }^{\circ}\text{C}$ and at a flow rate of $100\text{ L}\cdot\text{h}^{-1}$.

Figure 19 shows the influence of compressor power in Mode 3a with an HTF flow rate of $100\text{ L}\cdot\text{h}^{-1}$ and inlet temperature at $12\text{ }^{\circ}\text{C}$. Hereby the total cold energy stored at compressor powers of 15%, 30%, and 45% when steady state conditions are attained is about 5 kJ, 140 kJ, and 145 kJ, respectively. The time required to partially charge the PCM and attain thermal equilibrium was about 27 min, 28 min, 45 min for compressor powers of 15%, 30%, and 45%, respectively. As mentioned above, thermal equilibrium was not attained at 60% compressor power, while experimentation at compressor power of 75% was not feasible.

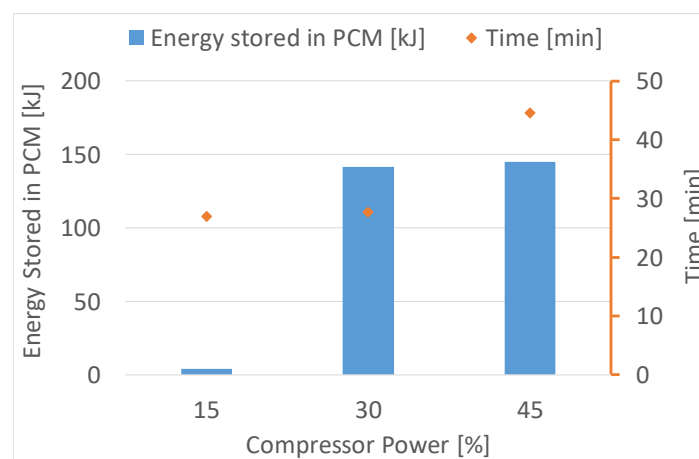


Figure 19. Influence of compressor power on the total cold energy stored in the PCM and time to reach thermal equilibrium for HTF inlet temperature of $12\text{ }^{\circ}\text{C}$ and at a flow rate of $100\text{ L}\cdot\text{h}^{-1}$.

The instantaneous cold energy and the final cold energy stored in the PCM at thermal equilibrium are shown in Figures 20 and 21, respectively. Both figures show the influence of the HTF flow rate on

the PCM in Mode 3a with compressor power at 30% and HTF inlet temperature at 12 °C. It is observed that the higher the flow rate the faster the thermal equilibrium is attained. Moreover, the cold energy stored in the PCM at equilibrium is observed to be lower for higher HTF flow rates.

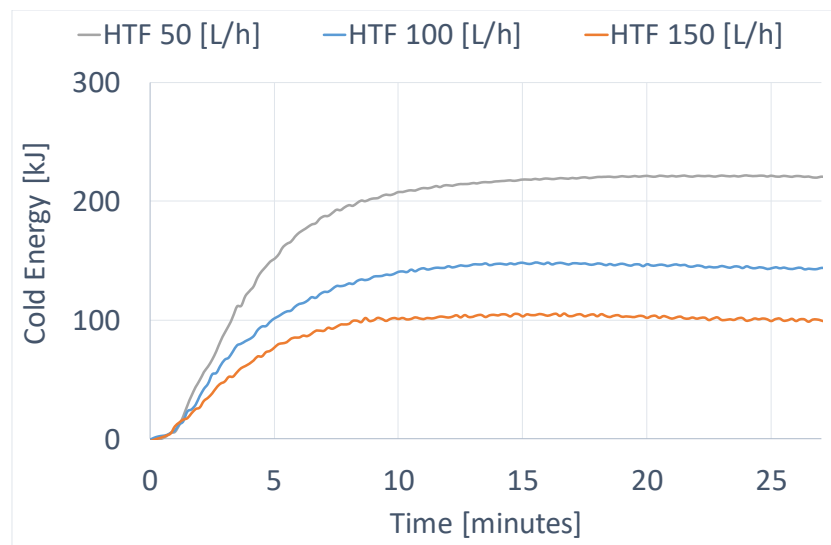


Figure 20. Influence of HTF flow rate on the instantaneous cold energy stored in the PCM in Mode 3a for HTF inlet temperature of 12 °C.

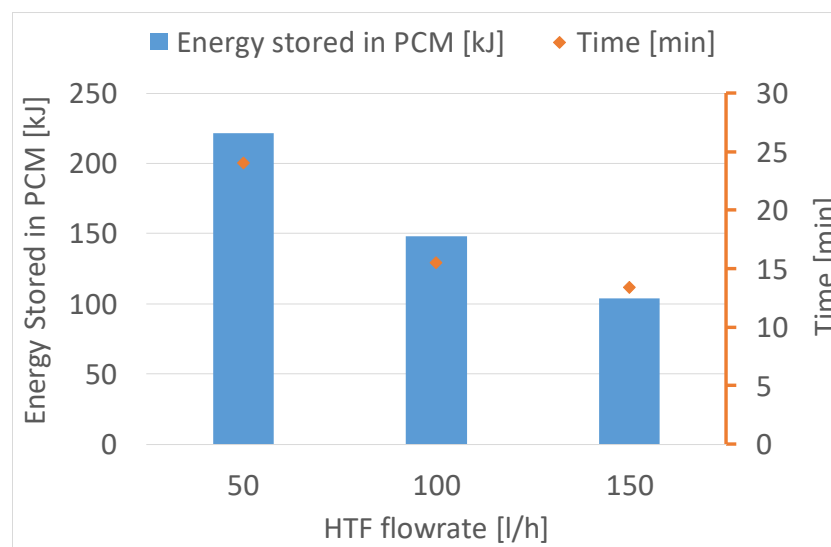


Figure 21. Influence of HTF flow rate on the total cold energy storage in the PCM and time to reach equilibrium for HTF inlet temperature at 12 °C.

3.3.2. Mode 3b: Simultaneous Charging and Discharging of the RPW-HEX with the PCM Initially Completely Charged

Temperature Profiles during the Simultaneous Charging and Discharging of the PCM

Regarding Mode 3b, the experimental conditions were similar to those in Mode 3a, except that the PCM was initially completely charged at −4 °C. Only experiments performed at compressor power at 15% were feasible, as shown in Table 9. Figure 22 shows the temperature profile in Mode 3b for the experiments performed at compressor power of 15%, with the HTF inlet temperature at 12 °C, and for HTF flow rates at 50 L·h^{−1}, 100 L·h^{−1}, and 150 L·h^{−1}. In this case, the whole cooling capacity of the refrigerant is used right from the beginning to cool down the HTF. Moreover, the HTF

was also cooled down by the PCM that also discharges part of the cold energy initially stored until steady state conditions are reached. At low HTF flow rates, PCM located at the top and middle parts of the RPW-HEX undergoes phase change and attains a temperature well above the phase change temperature, while PCM at the bottom part of the RPW-HEX remains completely or partially charged when thermal equilibrium is reached.

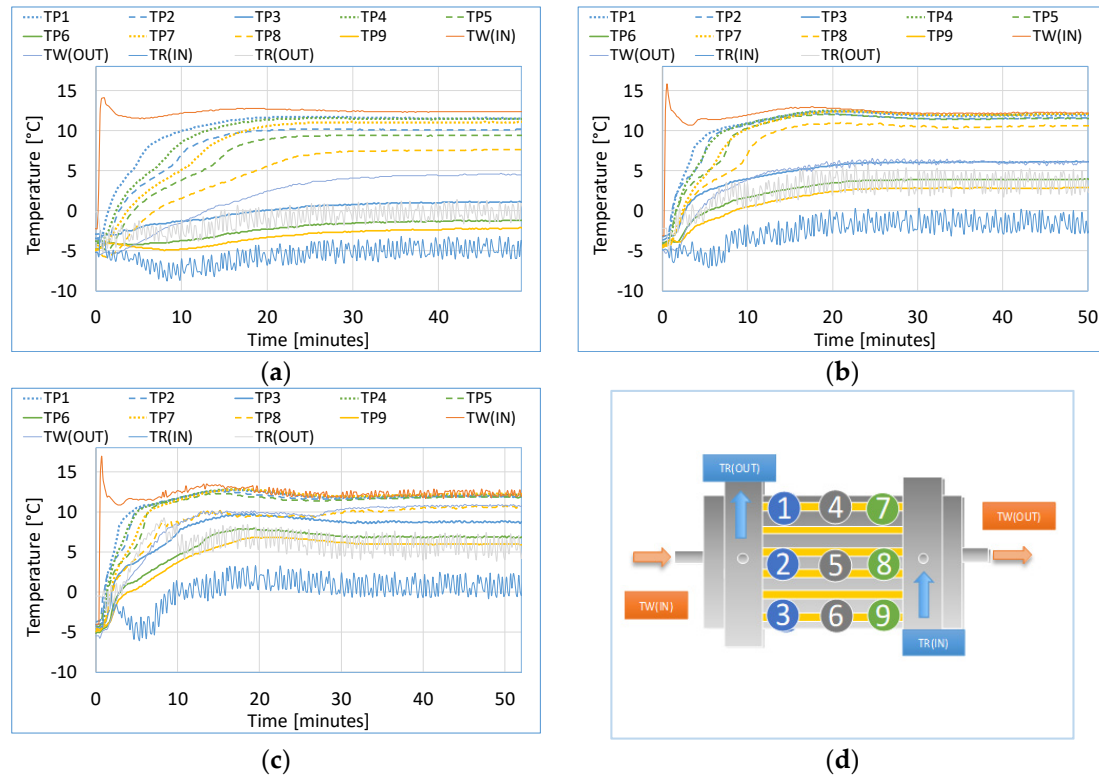


Figure 22. PCM temperature profile in Mode 3b for compressor power of 15%, with the HTF inlet temperature at 12 °C and flow rate of (a) 50 L·h⁻¹, (b) 100 L·h⁻¹, (c) 150 L·h⁻¹ and (d) position of the sensors. Dotted lines denote PCM temperature at top level, dashed lines at middle level, and solid lines at the bottom.

Instantaneous Cold Energy Stored in PCM, Total Cold Energy Storage and Time to Reach Equilibrium

Figures 23 and 24 show the influence of the HTF flow rate on the cold energy stored in PCM in Mode 3b with compressor power at 15%, with the HTF inlet temperature at 12 °C. Figure 23 shows that for the higher HTF flow rate the slope of the curve is steeper, meaning that the cold energy discharge rate is higher because of the higher heat capacity of the HTF leading to higher mean temperature difference between the PCM and the HTF and possibly also because of an increase in the heat transfer coefficient on the HTF side.

Figure 24 shows the total cold energy available in the PCM during thermal equilibrium and the time required to reach steady state conditions. The lower the HTF flow rate the higher the cold energy available at thermal equilibrium. The PCM was observed to be discharged from the initial cold energy available of about 290 kJ to about 76 kJ, 30 kJ, and 4 kJ in 30 min, 24 min, and 18 min by the HTF at 50 L·h⁻¹, 100 L·h⁻¹, and 150 L·h⁻¹, respectively. A similar behaviour to Mode 3a was observed with regards to the influence of the HTF flow rate on the total cold energy stored in the PCM when steady state conditions are attained. However, the influence of the compressor power on the cold energy could not be compared with Mode 3a because in Mode 3b only one compressor power (15%) was possible to be experimentally tested.

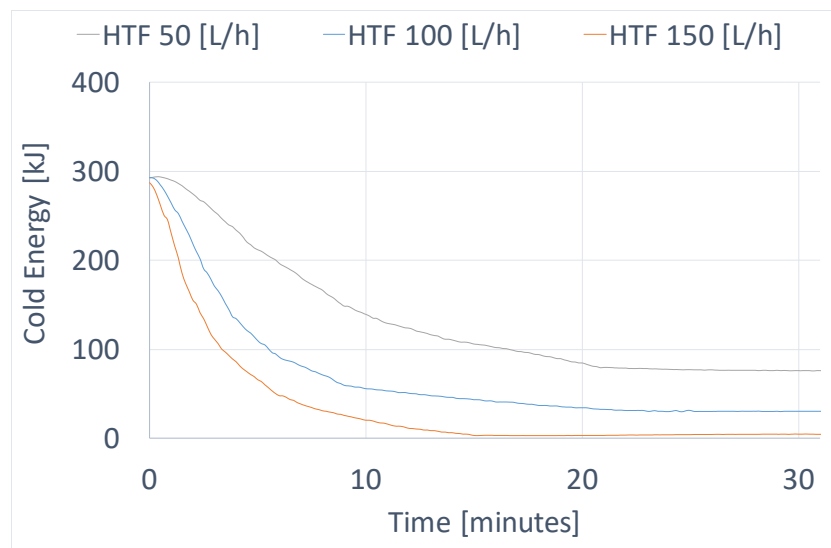


Figure 23. Influence of the HTF flow rate on the instantaneous cold energy stored in the PCM in Mode 3b with the HTF inlet temperature at 12 °C.

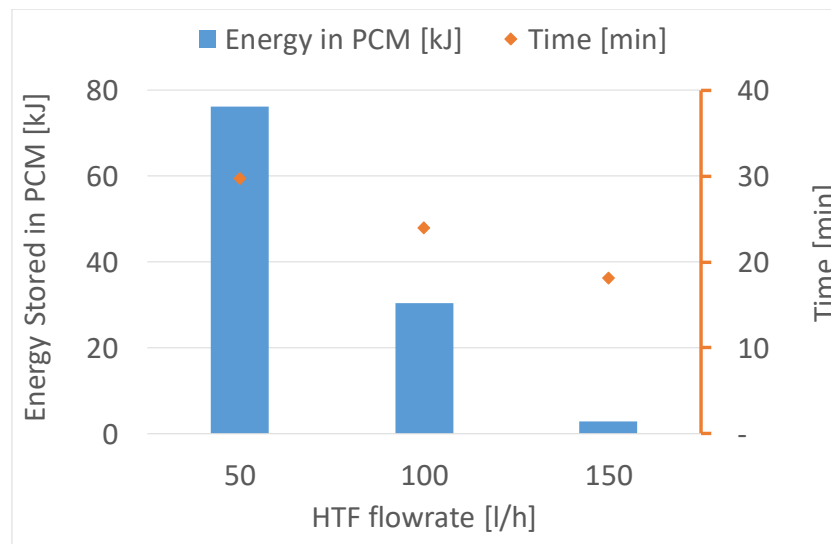


Figure 24. Influence of the HTF flow rate on the total cold energy stored in the PCM and time to reach equilibrium in Mode 3b with the HTF inlet temperature at 12 °C.

4. Discussion

This paper presents the results of a set of experiments performed with an innovative refrigerant-PCM-water heat exchanger as the evaporator of a standard vapour compression refrigeration system with variable cooling capacity. Three distinct operating modes were tested: charging, discharging, and simultaneous charging and discharging. In PCM charging and discharging modes, the RPW-HEX acts as a TES tank while in simultaneous charging and discharging mode it acts as a heat exchanger between the refrigerant and the HTF. The parameters analysed in all experiments were the PCM temperature profiles, the cold energy stored in the PCM, the energy charging or discharging rate of the PCM, and the duration of the processes in the three modes.

In the charging mode (Mode 1), different compressor powers ranging from 15% to 75% with regards to the maximum power capacity were tested for a fixed evaporation set-point of −10 °C. The results showed that a complete PCM charging was not possible, regardless the compressor cooling power. This is because of the stratification of PCM temperatures which makes it practically impossible to cool down the PCM located at the top part of the RPW-HEX well below the solidification temperature

of around 5 °C. A complete charging could still be possible if a lower evaporation set-point and a low compressor power were used, but this option is not attractive from a practical point of view. The duration of the charging process was considerably reduced from around 32 min to 3 min by increasing the compressor power from 15% to 75%. Nevertheless, the cold energy stored did not depend considerably on the compressor power, and the maximum amount of 294 kJ of cold energy stored in the PCM was achieved at a relatively low compressor power of only 30%. In spite of this, the charging at 60% compression power could be preferred because the charging duration is reduced by 60% with respect to the duration at 30% compressor power, while the reduction of the cold energy stored in the PCM is of only 7%.

In the discharging mode (Mode 2), different HTF inlet temperatures (9 °C, 12 °C, and 15 °C) and also different flow rates (50 L·h⁻¹, 100 L·h⁻¹, and 150 L·h⁻¹) were tested for the PCM initially completely charged. The results showed that the discharging duration decreased from 25 min to 9 min by increasing the HTF flow rate from 50 L·h⁻¹ to 150 L·h⁻¹ at constant HTF inlet temperature of 12 °C because of an increase in the heat transfer rate from 0.2 kW to 0.55 kW, respectively. Both the discharging duration and the heat transfer rate vary from 18 min to 8 min and from 0.3 kW to 0.65 kW by varying the inlet HTF temperature from 9 °C to 15 °C, respectively. Moreover, the PCM temperature profile showed a stratification of the HTF inside the RPW-HEX, with a temperature difference between the top and bottom parts of the PCM around 3 °C.

In the simultaneous charging and discharging mode (Mode 3), two different cases were considered: Mode 3a, for which the PCM was initially completely discharged (liquid state), and Mode 3b, for which the PCM was initially completely charged (solid state). Compressor powers between 15% and 75% and HTF flow rates of 50 L·h⁻¹, 100 L·h⁻¹, and 150 L·h⁻¹ were tested, with a fixed HTF inlet temperature of 12 °C. Not all planned experiments were feasible in practice since the evaporation temperature set-point was achieved before any part of the PCM could be charged, being the only feasible tests in Mode 3b the ones performed at a compressor power of 15%. This is one of the drawbacks related to the direct implementation of the RPW-HEX in the refrigeration system, which needs to be further analysed in more detail in future research. The results showed that, after an initial transient phase during which the PCM was either charged by the refrigerant (Mode 3a) or discharged by the HTF (Mode 3b), steady state conditions, characterised by thermal equilibrium between the refrigerant, PCM, and HTF, were achieved in both Modes 3a and 3b. When steady state was attained, the PCM reached a state of partial charge, in which only some parts of the PCM were in solid state. The cold energy stored in the PCM in steady state strongly depended on the HTF flow rate. The higher the HTF flow rate, the lower the energy stored and the shorter the time to reach the steady state. For instance, the results of the experiments performed in Mode 3b, in Figure 24, show that at a compressor power of 15% the cold energy stored in the PCM decreased from 76 kJ to only 4 kJ by increasing the HTF flow rate from 50 L·h⁻¹ to 150 L·h⁻¹. The cold energy stored in the PCM is also influenced by the compressor power according to the results of the experiments performed in Mode 3a, in which the energy increased from about 5 kJ to 145 kJ by increasing the compressor power from 15% to 45%. Moreover, a large temperature gradient throughout the PCM along the vertical direction was observed in both Mode 3a and 3b, being the temperature at the top of the RPW-HEX up to 20 °C higher than at the bottom.

Since the RPW-HEX was designed to contain seven sections (blocks), defined by different geometry and material distribution, and energy storage capacities the study presented in this paper can only be considered as a preliminary analysis aimed at presenting the novel concept and assessing the behaviour only of the PCM located at the central section (block A) of the RPW-HEX, as shown in Figure 5. However, some of the drawbacks such as temperature stratification, low cold storage capacity, and impossibility of attaining stable operating conditions should also be analysed in detail in future research. Other aspects such as the size, the influence of the auxiliary parts of the RPW-HEX, and the effect of the PCM integration on the performance of the refrigeration system as compared to a more traditional heat exchanger without PCM will also be investigated in future research.

5. Conclusions

This paper shows that the suggested innovative RPW-HEX has the ability to be used as a latent heat energy storage component in refrigeration systems to store the excess cold energy and discharge it at a later time. Based on the parameters studied, it is concluded that, though working at higher compressor power reduces the charging duration of the PCM, the stratification is higher leading to a part of the PCM not to solidify when the evaporator set-point temperature is achieved. During the discharging process, the stratification is higher for higher HTF inlet temperature and lower HTF flow rates. When operating as a heat exchanger (Mode 3), the RPW-HEX can initially either store or release energy depending on the initial PCM temperature and boundary conditions, until thermal equilibrium conditions are reached. In this case, the RPW-HEX acts as a heat exchanger, although it has the advantage of acting as a buffer due to the energy stored in the PCM. Care must be taken when selecting the appropriate values of the key parameters to adjust to the operating and boundary conditions imposed on the system, especially when operating as a heat exchanger (Mode 3) due to the greater number of parameters involved in the process. Furthermore, in future studies it seems essential to investigate the influence of the other parts and key characteristics of the RPW-HEX on the PCM temperature distribution and system performance.

Author Contributions: Conceptualization, G.Z. and L.F.C.; methodology, B.D.M., D.V. and G.Z.; investigation, B.D.M., D.V. and E.B.; formal analysis, B.D.M., G.Z. and L.F.C.; writing—original draft preparation, B.D.M. and D.V.; writing—review and editing, E.B., G.Z. and L.F.C.; supervision, L.F.C. and G.Z.; project administration, L.F.C.; funding acquisition, L.F.C. All authors have read and agreed to the published version of the manuscript.

Funding: This project has received funding from the European Union's Horizon 2020 research and innovation programme under grant agreement No. 768824 (HYBUILD). This work was partially funded by the Ministerio de Ciencia, Innovación y Universidades de España (RTI2018-093849-B-C31—MCIU/AEI/FEDER, UE) and by the Ministerio de Ciencia, Innovación y Universidades—Agencia Estatal de Investigación (AEI) (RED2018-102431-T). This work is partially supported by ICREA under the ICREA Academia programme.

Acknowledgments: The authors would like to thank the Catalan Government for the quality accreditation given to their research group (2017 SGR 1537). GREiA is certified agent TECNIO in the category of technology developers from the Government of Catalonia. Boniface Dominick Mselle would like to thank Programa Santander Predoc UdL for his research fellowship.

Conflicts of Interest: The authors declare no conflicts of interest. The funders had no role in the design of the study; in the collection, analyses, or interpretation of data; in the writing of the manuscript, or in the decision to publish the results.

References

1. Coulomb, D.; Dupont, J.; Pichard, A. *The Role of Refrigeration in the Global Economy*; International Institute of Refrigeration: Paris, France, 2015.
2. International Energy Agency. *World Energy Outlook 2019*; International Energy Agency: Paris, France, 2019.
3. United Nations Framework Convention On Climate Change. *Paris Agreement*; United Nations Framework Convention On Climate Change: Paris, France, 2015.
4. Cabeza, L.F.; Urge-Vorsatz, D.; McNeil, M.A.; Barreneche, C.; Serrano, S. Investigating greenhouse challenge from growing trends of electricity consumption through home appliances in buildings. *Renew. Sustain. Energy Rev.* **2014**, *36*, 188–193. [[CrossRef](#)]
5. Soares, N.; Bastos, J.; Pereira, L.D.; Soares, A.; Amaral, A.R.; Asadi, E.; Rodrigues, E.; Lamas, F.B.; Monteiro, H.; Lopes, M.A.R.; et al. A review on current advances in the energy and environmental performance of buildings towards a more sustainable built environment. *Renew. Sustain. Energy Rev.* **2017**, *77*, 845–860. [[CrossRef](#)]
6. James, C.; Onarinde, B.A.; James, S.J. The Use and Performance of Household Refrigerators: A Review. *Compr. Rev. Food Sci. Food Saf.* **2017**, *16*, 160–179. [[CrossRef](#)]
7. Mastani Joybari, M.; Haghighat, F.; Moffat, J.; Sra, P. Heat and cold storage using phase change materials in domestic refrigeration systems: The state-of-the-art review. *Energy Build.* **2015**, *106*, 111–124. [[CrossRef](#)]
8. Cengel, Y.A.; Boles, M.A. *Thermodynamics: An Engineering Approach*, 7th ed.; McGraw-Hill: New York, NY, USA, 2010.

9. Mehling, H.; Cabeza, L.F. *Heat and Cold Storage with PCM—An Up to Date Introduction into Basics and Applications*, 1st ed.; Springer: Berlin/Heidelberg, Germany, 2008.
10. Sharma, A.; Tyagi, V.V.; Chen, C.R.; Buddhi, D. Review on thermal energy storage with phase change materials and applications. *Renew. Sustain. Energy Rev.* **2009**, *13*, 318–345. [[CrossRef](#)]
11. Axell, M.; Bakker, M.; Landolina, S. Strategic Research Priorities for Cross-Cutting Technology. *Eur. Technol. Platf. Renew. Heat. Cool.* **2012**, *108*.
12. Cheng, W.L.; Mei, B.J.; Liu, Y.N.; Huang, Y.H.; Yuan, X.D. A novel household refrigerator with shape-stabilized PCM (Phase Change Material) heat storage condensers: An experimental investigation. *Energy* **2011**, *36*, 5797–5804. [[CrossRef](#)]
13. Wang, F.; Maidment, G.; Missenden, J.; Tozer, R. The novel use of phase change materials in refrigeration plant—Part 1: Experimental investigation. *Appl. Therm. Eng.* **2007**, *27*, 2893–2901. [[CrossRef](#)]
14. Cheng, W.; Ding, M.; Yuan, X.; Han, B.C. Analysis of energy saving performance for household refrigerator with thermal storage of condenser and evaporator. *Energy Convers. Manag.* **2017**, *132*, 180–188. [[CrossRef](#)]
15. Azzouz, K.; Leducq, D.; Gobin, D. Enhancing the performance of household refrigerators with latent heat storage: An experimental investigation. *Int. J. Refrig.* **2009**, *32*, 1634–1644. [[CrossRef](#)]
16. Azzouz, K.; Leducq, D.; Gobin, D. Performance enhancement of a household refrigerator by addition of latent heat storage. *Int. J. Refrig.* **2008**, *31*, 892–901. [[CrossRef](#)]
17. Copertaro, B.; Fioretti, R.; Principi, P. Experimental analysis on a novel air heat exchanger containing PCM (Phase change material) in a cold room. In *Proceedings of the Refrigeration Science and Technology*, Bucharest, Romania, 22–25 June 2016; pp. 142–150.
18. Rubitherm. *Rubitherm RT-LINE Datasheet*; Rubitherm: Berlin, Germany, 2018.
19. Zsembinszki, G.; Fernández, A.G.; Cabeza, L.F. Selection of the appropriate phase change material for two innovative compact energy storage systems in residential buildings. *Appl. Sci.* **2020**, *10*, 2116. [[CrossRef](#)]
20. The Dow Chemical Company. *The Dow Chemical Company Dowtherm SR-1*; The Dow Chemical Company: Bellevue, WA, USA, 2020.



© 2020 by the authors. Licensee MDPI, Basel, Switzerland. This article is an open access article distributed under the terms and conditions of the Creative Commons Attribution (CC BY) license (<http://creativecommons.org/licenses/by/4.0/>).